Am J Physiol Heart Circ Physiol 305: H1752–H1760, 2013.
First published October 4, 2013; doi:10.1152/ajpheart.00514.2013.

Intrauterine growth restriction is associated with cardiac ultrastructural and gene expression changes related to the energetic metabolism in a rabbit model

Anna Gonzalez-Tendero,[1] Iratxe Torre,[1,2] Patricia Garcia-Canadilla,[1,3] Fátima Crispi,[1,2,4] Francisco García-García,[5,6,7] Joaquin Dopazo,[5,6,7] Bart Bijnens,[3] and Eduard Gratacós[1,2,4]

[1]*Fetal and Perinatal Medicine Research Group, Institut d'Investigacions Biomèdiques August Pi i Sunyer, University of Barcelona, Barcelona, Spain;* [2]*Centro de Investigación Biomédica en Red de Enfermedades Raras, Hospital Clinic-University of Barcelona, Barcelona, Spain;* [3]*ICREA-PhySense, N-RAS, Universitat Pompeu Fabra, Barcelona, Spain;* [4]*Department of Maternal-Fetal Medicine, Institut Clínic de Ginecologia, Obstetrícia i Neonatologia, Barcelona, Spain;* [5]*Bioinformatics Department, Centro de Investigación Principe Felipe, Valencia, Spain;* [6]*Functional Genomics Node, INB, Centro de Investigación Principe Felipe, Valencia, Spain; and* [7]*Centro de Investigación Biomédica en Red de Enfermedades Raras, Centro de Investigación Principe Felipe, Valencia, Spain*

Submitted 3 July 2013; accepted in final form 28 September 2013

Gonzalez-Tendero A, Torre I, Garcia-Canadilla P, Crispi F, García-García F, Dopazo J, Bijnens B, Gratacós E. Intrauterine growth restriction is associated with cardiac ultrastructural and gene expression changes related to the energetic metabolism in a rabbit model. *Am J Physiol Heart Circ Physiol* 305: H1752–H1760, 2013. First published October 4, 2013; doi:10.1152/ajpheart.00514.2013.—Intrauterine growth restriction (IUGR) affects 7–10% of pregnancies and is associated with cardiovascular remodeling and dysfunction, which persists into adulthood. The underlying subcellular remodeling and cardiovascular programming events are still poorly documented. Cardiac muscle is central in the fetal adaptive mechanism to IUGR given its high energetic demands. The energetic homeostasis depends on the correct interaction of several molecular pathways and the adequate arrangement of intracellular energetic units (ICEUs), where mitochondria interact with the contractile machinery and the main cardiac ATPases to enable a quick and efficient energy transfer. We studied subcellular cardiac adaptations to IUGR in an experimental rabbit model. We evaluated the ultrastructure of ICEUs with transmission electron microscopy and observed an altered spatial arrangement in IUGR, with significant increases in cytosolic space between mitochondria and myofilaments. A global decrease of mitochondrial density was also observed. In addition, we conducted a global gene expression profile by advanced bioinformatics tools to assess the expression of genes involved in the cardiomyocyte energetic metabolism and identified four gene modules with a coordinated over-representation in IUGR: oxygen homeostasis (GO: 0032364), mitochondrial respiratory chain complex I (GO:0005747), oxidative phosphorylation (GO: 0006119), and NADH dehydrogenase activity (GO:0003954). These findings might contribute to changes in energetic homeostasis in IUGR. The potential persistence and role of these changes in long-term cardiovascular programming deserves further investigation.

cardiomyocyte intracellular organization; energetic metabolism; fetal cardiac programming; intracellular energetic units; intrauterine growth restriction

INTRAUTERINE GROWTH RESTRICTION (IUGR), due to placental insufficiency, affects up to 7–10% of pregnancies and is a major cause of perinatal mortality and long-term morbidity (1). Low birth weight, most likely due to IUGR, is strongly associated with increased risk of cardiovascular mortality in adulthood (7). This association is thought to be mediated through fetal cardiovascular programming. IUGR fetuses suffer from a chronic restriction of oxygen and nutrients (47), which triggers the initiation of a variety of adaptive structural (12, 14, 46, 51) and metabolic responses (25) due to a pressure/volume overload and, subsequently, with the objective of providing a more efficient myocardial performance. As a consequence, IUGR fetuses and newborns show signs of cardiovascular remodeling and altered function (21, 13, 14).

The effect of hypoxia and nutrient restriction during pregnancy in cardiac development and function has been previously studied, demonstrating the association of IUGR to a cardiac remodeling. Maternal hypoxia has been related to changes in cardiac structure and function (37, 38, 49), increased cardiac collagen content (50), and changes in cardiomyocyte proliferation and apoptosis (6, 28) and to long-term effects increasing cardiac susceptibility to ischemia-reperfusion injury by causing changes on myocardial energetic metabolism (39, 55). However, the underlying events of cardiac remodeling in IUGR at subcellular scale still remain poorly understood. The heart is an organ with high-energy requirements in the form of ATP to ensure proper functioning (29). Efficient energetic homeostasis depends on the correct arrangement of subcellular organelles. A close spatial interaction between mitochondria and the sarcomere contractile filaments is essential to ensure adequate and quick transportation of ATP. This is reached by the intracellular energetic units (ICEUs), which are structural and functional units, consisting of mitochondria located at the level of the sarcomeres between Z-lines interacting with surrounding myofilaments, sarcoplasmic reticulum, cytoskeleton, and cytoplasmic enzymes, that promote an endogenous cycling of adenine nucleotides between mitochondria and ATPases (40, 44, 45). Alterations in ICEUs arrangement together with an impaired local energetic regulation of the main cardiac ATPases have been described in cardiac pathophysiological processes (24). In addition, cardiomyocyte energetic homeostasis is regulated by a complex interaction of molecular pathways, mainly involving energy production through oxidative phosphorylation in the mitochondria (48). It has been widely described that disruption of mitochondrial oxidative phosphorylation plays a critical role in the development of heart failure (26, 35, 52). The oxidative phosphorylation takes place in the mitochondrial electron transport chain. It is composed of five complexes; in the complex I the enzyme NADH dehydrogenase catalyzes the reaction (2). Deficiencies in complex I

Address for reprint requests and other correspondence: E. Gratacós, Dept. of Maternal-Fetal Medicine, ICGON, Hospital Clinic. Sabino de Arana, 1 08028 Barcelona, Spain (e-mail: gratacos@clinic.ub.es).

function have been observed in dilated cardiomyopathy and in failing myocardium (41).

The goal of the present work was to evaluate the impact of chronic oxygen and nutrient restriction during a critical period for cardiac development, as present in IUGR, with regard to cardiomyocyte intracellular organization and gene expression of key pathways for energetic metabolism. For this purpose, the cardiomyocyte intracellular organization was studied by transmission electron microscopy. Additionally, the functional interpretation of the global gene expression profile was studied by means of advanced bioinformatics tools. The data presented here show changes in the cardiomyocyte intracellular organization in IUGR, specifically affecting ICEUs, together with an abnormal uprepresentation of blocks of genes acting together in a coordinated way, related to the cardiac oxygen homeostasis and energy production.

MATERIALS AND METHODS

Animal Model

New Zealand white rabbits were provided by a certified breeder. Dams were housed for 1 wk before surgery in separate cages on a reversed 12-h/12-h light cycle. Animals were fed a diet of standard rabbit chow and water ad libitum. Animal handling and all procedures were performed in accordance to applicable regulations and guidelines and with the approval of the Animal Experimental Ethics Committee of the University of Barcelona.

Six New Zealand white pregnant rabbits were used to reproduce a model of IUGR, following the method previously described (16, 17). At 25 days of gestation, selective ligature of uteroplacental vessels was performed as previously described (16, 17). Briefly, tocolysis (progesterone 0.9 mg/kg im) and antibiotic prophylaxis (Penicillin G 300.000 UI iv) were administered before surgery. Ketamine (35 mg/kg) and xylazine (5 mg/kg) were given intramuscularly for anesthesia induction. Inhaled anesthesia was maintained with a mixture of 1–5% isoflurane and 1–1.5 l/min oxygen. After a midline laparatomy, both uterine horns were exteriorized. The number of gestational sacs from each horn were counted and numbered. Pregnant rabbits have between 4 and 7 gestational sacs per horn. At random, one horn was assigned as the IUGR horn and the other horn was considered as the normal control growth. In all gestational sacs from the horn assigned as IUGR, a selective ligature of the 40–50% of the uteroplacental vessels was performed. No additional procedure was performed in the horn assigned as control. After the procedure, the abdomen was closed and animals received intramuscular meloxicam 0.4 $mg \cdot kg^{-1} \cdot 24\ h^{-1}$ for 48 h, as postoperative analgesia. Five days after surgery, at 30 days of gestation, a caesarean section was performed under the same anesthetic procedure and all living rabbit kits and their placentas were identified and weighted. Kits were anesthetized with an injection of ketamine and xylazine. After surgical removal from the chest cavity, hearts for gene expression analysis were immediately snap-frozen and stored at −80°C until the moment of use. Hearts for transmission electron microscopy imaging were processed as described in *Tissue processing*.

Electron Microscopy

Tissue processing. Hearts from 3 control and 3 IUGR rabbit fetuses, each control-IUGR pair coming from a different litter, were arrested in an ice-cold Ca^{2+}-free phosphate saline buffer immediately after surgical removal from the chest cavity. Random areas of left ventricle were dissected and cut into small pieces. Approximately 10 pieces from each left ventricle were incubated with 2% parafomaldehyde and 2.5% glutaraldehyde in phosphate buffer (PB) during 24 h at 4°C. Tissue pieces were then washed with PB and postfixed with 1% osmium tetroxide in PB containing 0.8% potassium ferricyanide at 4°C for 2 h. Next, samples were dehydrated in acetone, infiltrated with Epon resin during 2 days, embedded in the same resin, and polymerized at 60°C during 48 h. Semi-thin 500-nm sections were made to confirm the longitudinal orientation of cardiac sarcomeres under light microscope. Subsequently, 50-nm ultra-thin sections were cut using a Leica UC6 ultramicrotome (Leica Microsystems, Vienna, Austria) and mounted on Formvar-coated copper grids. Sections were stained with 2% uranyl acetate in water and lead citrate. Tissue sections were imaged using a JEM-1010 electron microscope (Jeol, Japan) equipped with a charge-coupled device camera Megaview III and the AnalySIS software (Soft Imaging System GmbH).

Morphological analysis. Morphological analysis of intracellular cardiomyocyte organization was performed in two randomly chosen left ventricle tissue pieces, from each subject. For each tissue piece, 50-nm ultra-thin sections were obtained from two ventricular areas separated 1 μm of distance. Images were taken at 20,000× magnification when an area containing longitudinal myofilaments surrounded by a mitochondrial network was observed. In this study, micrographs with disrupted mitochondria, disrupted sarcomeres or transversal or oblique orientation of sarcomeres were excluded from the quantification. Electron micrographs were taken and quantified in a blinded fashion and by one researcher (A. Gonzalez-Tendero). Images were analyzed from three viewpoints.

General cardiomyocyte cytoarchitecture: volume density estimation. The volume densities of myofilaments, mitochondria, and cytoplasm were estimated in 10 electron micrographs acquired from each heart. For this purpose, a grid in which each line intersection served as a sample point was generated on each image using ImageJ (36), according to standard stereological methods (20). Volume densities of the different structures were calculated by counting the number of points hitting the studied structures divided by the total number of points hitting the section, using a grid size of 0.02 a.u.

Mitochondria: area and number. The area of individual mitochondria was determined from 193 mitochondria in each study group. Individual mitochondria were delineated, and their area was measured using the AnalySIS software. The number of mitochondria was counted by using 10 randomly chosen images from each heart as previously described (22).

ICEUs arrangement. The cytoplasmic area and the mean distance between mitochondria and myofilaments within ICEUs were measured by delineating the area of cytoplasm existing between two consecutive z-disks and the immediately adjacent mitochondria, as shown in Fig. 1, using a custom-made GUI (Graphical User Interface) designed in MatLab (30). The area was automatically calculated, and the mean distance between mitochondria and myofilaments within

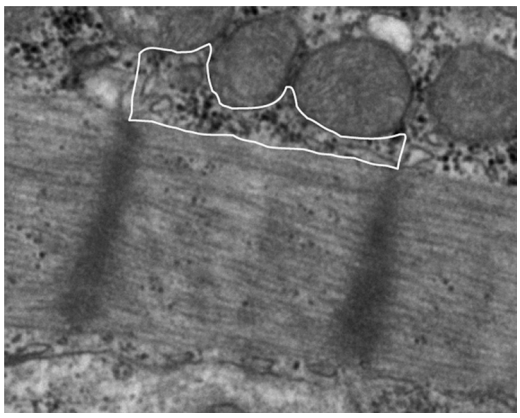

Fig. 1. Electron micrograph showing an example of the delineation used to automatically quantify the area of cytoplasm and the mean distance between mitochondria and myofilaments within intracellular energetic units (ICEUs).

ICEUs was obtained by evaluating the Euclidean distance of the delineated region (11). A total of 169 ICEUs were analyzed in the control group, whereas 154 ICEUs were analyzed in the IUGR group, obtained from 10 to 15 electron micrographs from each heart. We analyzed all the ICEUs found in the transmission electron microscopy images. However, ICEUs were discarded from the quantification when they were not clear or blurred or if the limits to mitochondria were not sharp enough.

Gene Set Expression Analysis

Gene expression microarray. The IUGR-gene expression profile was analyzed in 6 control and 6 IUGR rabbit fetuses, each control-IUGR pair coming from a different litter. In this study, special attention was paid to the expression profile of groups of genes related to energetic metabolism. Total RNA was isolated from 40 mg of each left ventricle. The extraction protocol was a combination of TRIzol as reagent and the RNeasy Mini kit (Qiagen). For each sample included in the study, the total amount of RNA was always above 25 μg with homogenous profile, showing an RNA integrity number between 9.3 to 9.9 (analyzed with RNA 6000 Nano and Bioanalyzer 2100; Agilent). Next, 500 ng of total RNA from each sample were labeled with the Quick Amp One-color Labelling kit (Agilent) and fluorochrome Cy3. Efficiency of labeling (Cy3pmol/μg) was analyzed using a Nanodrop spectrophotometer to check that values were above the minimum requirements (>1.65 μg and >9.0 pmols Cy3/μg). Additionally, a RNA 6000 Nano mRNA assay in the Bioanalyzer 2100 was done to assess that all the samples show a comparable profile and fragments size was as expected (200–2,000 bp). Then, 1,650 μg of RNA obtained from each labeled sample were hybridized during 17 h at 65°C with a Rabbit Microarray (Agilent Microarray Design ID 020908) containing 43,803 probe sequences obtained from the rabbit genome. All probe sequences included in the microarray were based on rabbit (*Oryctolagus cuniculus*) public transcript data. Finally, hybridization was quantified at 5 μm resolution (Axon 4000B scanner). Data extraction was done using Genepix Pro 6.0 software, and results were subjected to bioinformatics analysis.

Gene set analysis. Gene set analysis was carried out for the Gene Ontology (GO) terms using the FatiScan (3) algorithm, implemented in the Babelomics suite (4). This method detects significantly up- or downregulated blocks of functionally related genes in lists of genes ordered by differential expression. FatiScan can search for modules of genes that are functionally related by different criteria such as common annotations like GO terms.

The FatiScan algorithm studies the distribution of functional terms across the list of genes coming from the microarray experiment, extracting significantly under- and over-represented GO terms in a set of genes. GO terms were grouped in three categories: *1*) cellular components, that refer to the place in the cell where a gene product is active; *2*) biological processes, which refer to a biological objective to which a gene or gene product contributes; and *3*) molecular functions that represent all the biochemical activities of a gene product. FatiScan uses a Fisher's exact test for 2 × 2 contingency tables for comparing two groups of genes and extracting a list of GO terms whose distribution among the groups is significantly different. Given that many GO terms are simultaneously tested, the results of the test are corrected for multiple testing to obtain an adjusted *P* value. FatiScan returns adjusted *P* values based on the False Discovery Rate (FDR) method (10). GO annotation for the genes in the microarray were taken from the Blast2GO Functional Annotation Repository web page (http://bioinfo.cipf.es/b2gfar/). The raw microarray data have been deposited in the Gene Expression Omnibus database under accession number GSE37860.

Statistical Analysis

Statistical analysis of the morphological study was performed with the statistical package SPSS 18.0. Data are expressed as means ± SD or median (interquartile range, IQR). Statistical significance of differences between experimental groups was compared with an unpaired two-tailed *t*-test or Mann-Whitney test, depending whether variables followed a normal distribution. Differences were considered significant with probability values of $P < 0.05$. Statistical methods concerning gene expression analysis have been detailed in *Gene set analysis*.

RESULTS

Animal Model of IUGR: Fetal Biometry

Table 1 summarizes biometric outcome of the study groups. Birth weight, placental weigth, heart weight, crown-rump length, and abdominal girth decreased significantly in IUGR kits compared with normally growth kits. Additionally, heart-to-body weight ratio was increased in the IUGR group.

Morphological Analysis

General cardiomyocyte cytoarchitecture. Significant differences between IUGR and normally growth fetal myocardium could be observed regarding the arrangement of the intracellular components. A representative image of this is displayed in Fig. 2, *A* and *B*, showing that IUGR rabbits present a looser packing of mitochondria and an increased cytosolic space between mitochondria and myofilaments. Quantification of the volume densities of myofilaments, mitochondria, and cytoplasm is shown in Fig. 2*C*. Stereological examination of micrographs obtained from control and IUGR myocardium showed that the amount of myofilaments was not different between control and IUGR rabbits (mean 34.64 ± SD 4.04% in control vs. 34.74 ± 6.01% in IUGR; $P = 0.973$). On the other hand, changes in the relative volume occupied by mitochondria and cytoplasm were observed among control and IUGR myocardium. The relative volume occupied by mitochondria was significantly decreased in IUGR fetuses (34.59 ± 4.23% in control vs. 27.74 ± 5.28% in IUGR; $P = 0.032$), whereas the relative volume occupied by total cytoplasm was significantly increased under IUGR (30.77 ± 3.04% in control vs. 37.53 ± 4.97% in IUGR; $P = 0.018$). In this study we classified the cytoplasm into two categories according to its localization: *1*) cytoplasm located between mitochondria and myofilaments (ICEUs) and *2*) cytoplasm not located in the ICEUs, namely free cytoplasm. The cytoplasm existing within ICEUs was significantly increased under IUGR (6.47 ± 0.1.18% in control vs. 8.69 ± 1.75% in IUGR; $P = 0.027$). However, the free cytoplasm was not altered (24.31 ± 2.91% in control vs. 28.84 ± 5.27% in IUGR; $P = 0.095$).

Mitochondria: area and number. The average area of individual mitochondria as well as the number of mitochondria were quantified to test whether changes described in *General cardiomyocyte cyotarchitecture* could be due to changes in the mitochondrial size or number (Fig. 3). Results did not show statistically significant differences regarding the area of individual mitochondria

Table 1. *Biometry in experimental groups*

	Control	IUGR	*P* Value
Weight, g			
Birth	49.24 ± 8.03	29.76 ± 5.99	0.000*
Heart	0.43 ± 0.07	0.29 ± 0.07	0.001*
Heart/body, ×100	0.84 ± 0.12	1.02 ± 0.11	0.009*
Placenta	3.86 ± 1.06	2.23 ± 0.37	0.028*
Crown-rump length, mm	10.56 ± 0.46	8.94 ± 1.05	0.004*
Abdominal girth, mm	7.47 ± 0.93	6.38 ± 0.65	0.048*

Values are mean ± SD. IUGR, intrauterine growth restriction. *P value <0.05.

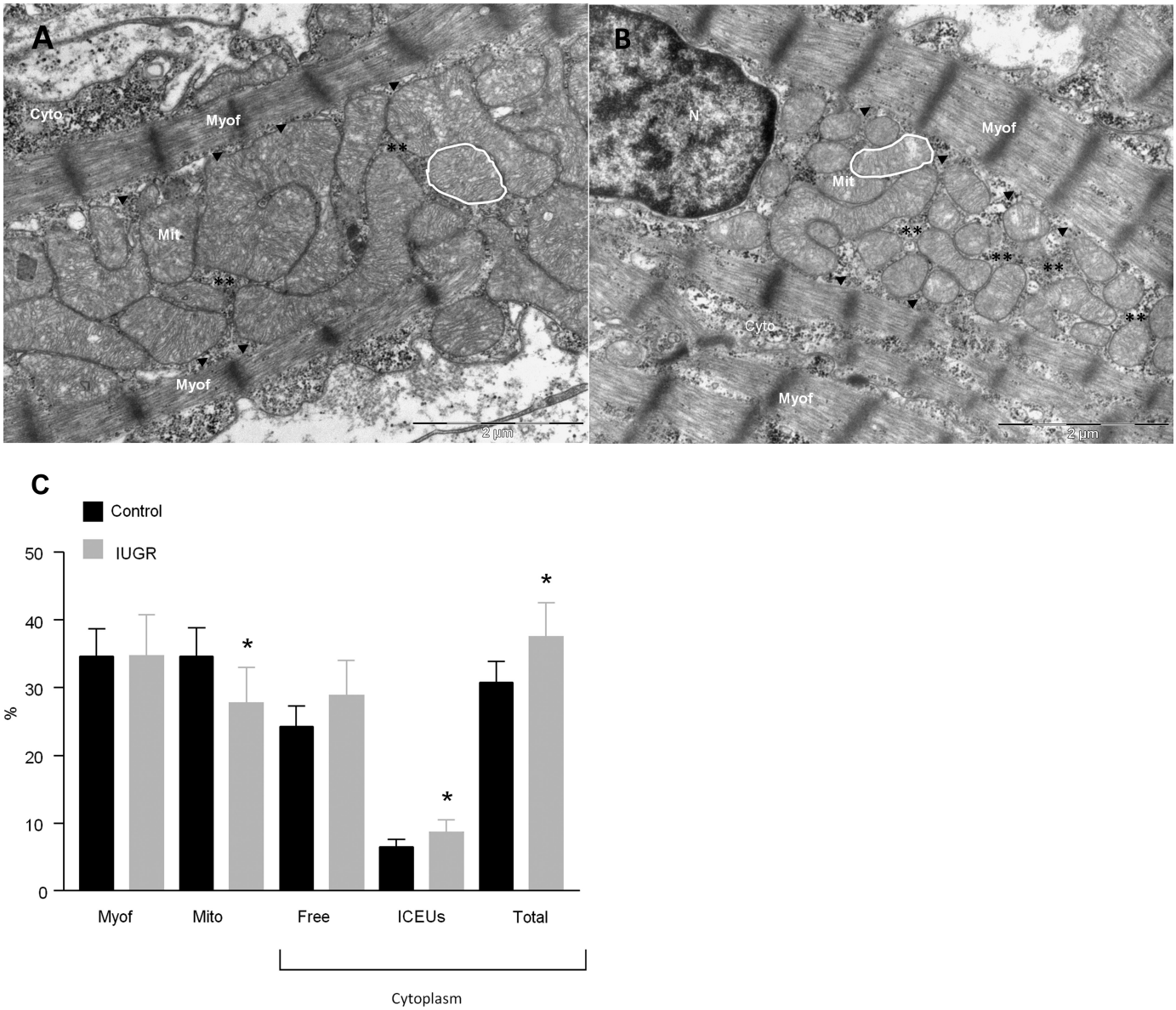

Fig. 2. Cytoarchitectural organization of cardiac myocytes. Representative micrographs show the typical organization of the intracellular space in control (*A*) and intrauterine growth restriction (IUGR; *B*) fetal cardiomyocytes. Although mitochondria are highly compacted and packed close to myofilaments in controls, they are looser packed, showing an increased cytosolic space both within the mitochondrial network (**) and between mitochondria and myofilaments (arrow heads) in IUGR. *C*: stereological measurements of fetal control and IUGR cardiomyocytes showing the relative volume occupied by myofilaments, mitochondria, free cytoplasm (Free), cytoplasm between mitochondria and myofilaments (ICEUs), and total cytoplasm (Total). *$P < 0.05$. Data in graphs are expressed as means ± SD. Magnification: 20,000×. Scale bar = 2 μm. Mit, mitochondria; Myof, myofilaments; Cyto, cytoplasm; N, nucleus.

(0.3094 ± 0.0595 μm^2 in control vs. 0.2407 ± 0.0176 μm^2 in IUGR; $P = 0.128$). Average number of mitochondria neither resulted to be different between control and IUGR hearts (27.47 ± 9.32 in control vs. 26.33 ± 8.06 in IUGR; $P = 0.627$).

ICEUs arrangement. The area and mean distance between mitochondria and myofilaments were automatically quantified (Fig. 4). Results showed that both the area of cytoplasm between mitochondria and myofilaments within ICEUs [median 120700 (IQR 87490–155500) nm^2 in control vs. 168600 (124100–236200) nm^2 in IUGR; $P = 0.015$; Fig. 4*E*] and the mean distance [105.7 (86.7–137.9) nm in control vs. 133.7 (104.7–182.3) nm in IUGR; $P = 0.037$; Fig. 4*F*] were significantly increased in IUGR rabbit myocardium.

Gene Set Expression Analysis

All experiments showed a good level of labeling and hybridization onto the Agilent microarray. Genes were ordered by differential expression between the two experimental conditions, and a ranked list with all genes of the experiment was obtained. We used the statistic of the statistical test for each gene, to order this list: genes at the top of list are more expressed in IUGR than in control group and genes at the bottom are more expressed in control than IUGR group. After analysis for a fold change higher than 0.5 and an adjusted *P* value lower than 0.05 (data not shown), there were not genes with significant differential expression. The output result of the

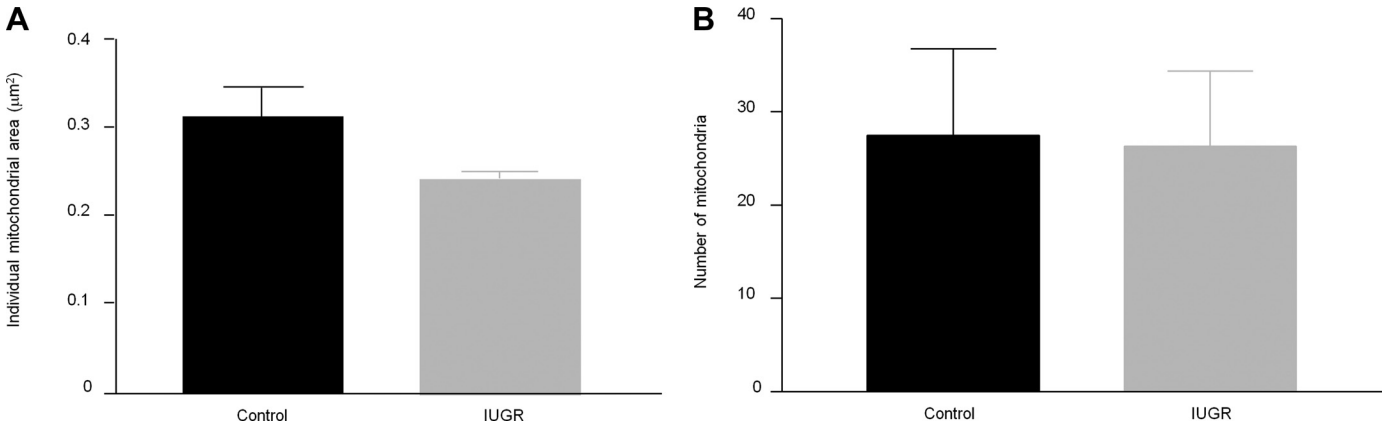

Fig. 3. Mitochondria area and number. *A*: average area of individual mitochondria, estimated delineating each mitochondria as shown in Fig. 2, *A* and *B*. *B*: average number of mitochondria. Data in graphs are expressed as means ± SD.

differential expression analysis (ranked list by the statistic of the test) was the input for the gene set analysis. On this full list of genes, Fatiscan detected groups of genes with the same expression pattern and sharing biological functions and extracted significantly under- and over-represented Gene Ontology terms in a set of genes after comparing two sub-lists of genes with different pattern of expression. The first list included genes more expressed in IUGR group, and the second, genes more expressed in the control group. Gene set analysis showed that IUGR subjects presented a statistically significant enrichment in groups of genes involved in energy production and cardiac energetic metabolism regulation (Table 2). Oxidative phosphorylation annotation (GO: 0006119, biological process) was found in 1.03% of the most upregulated genes in IUGR (list 1, more expressed in IUGR than control group), whereas only 0.17% of the most downregulated genes in IUGR contained the annotation (list 2, more expressed in control than IUGR group) (see Supplemental Material, Supplemental Table S. 1A). Similarly, the annotations for oxygen homeostasis (GO: 0032364, biological process) (Supplemental Table S. 1B), mitochondrial respiratory chain complex I (GO: 0005747, cellular component) (Supplemental Table S. 1C), and NADH dehydrogenase (GO: 0003954, molecular function) (Supplemental Table S. 1D) were found in 0.49%, 0.44%, and 0.35%, respectively, of the most upregulated genes in IUGR and only in 0.04%, 0%, and 0% of the most downregulated genes in IUGR, respectively. All P values were ≤ 0.001, and all adjusted P values were <0.08.

DISCUSSION

The study presented here shows an association between IUGR and a less organized intracellular arrangement of the cardiomyocyte organelles. The specific disarrangement of the ICEUs together with differences in the expression of key pathways for energy production suggest an impairment of the energetic metabolism under IUGR. This study can contribute to explain the process of fetal cardiac programming and the global contractile dysfunction previously described in IUGR fetuses and children (12, 13, 14).

The experimental IUGR model used in this study is based on the selective ligature of the uteroplacental vessels in pregnant rabbit at 25 days of gestation until 30 days of gestation. The model mimics IUGR in human pregnancy, since it induces a combined restriction of oxygen and nutrients, taking into account the role of the placenta (16, 17). Different gestational ages as well as different degrees of ligature severity were previously tested for this experimental IUGR model, with conclusions that the condition that best reproduced human IUGR due to placental insufficiency is the selective ligature of the 40–50% of the uteroplacental vessels at 25 days of gestation (16). It is known that in rabbits, complete organogenesis has been achieved at 19.5 days of gestation (9). The two previous statements together with the aim to reproduce late IUGR occurring in the third trimester of human pregnancy (which is mainly caused by placental and maternal vascular factors) lead to the rationale of the ligature from 25 to 30 days of gestation (16, 8). The severity of the experimental IUGR model reproducing human IUGR condition due to placental insufficiency, with regard to mortality rate and hemodynamic changes, has been previously described (16, 17). Cardiac function from IUGR kits is characterized by changes on cardiovascular Doppler parameters, with increased ductus venosus pulsatility index and increased isovolumetric relaxation time (17). Here we present the biometric changes induced by the selective ligature of 40–50% of the uteroplacental vessels, which result, as expected, in lower birth and heart weights, as well as decreased crown-rump length and abdominal girth. Additionally, an increase in heart to body weight is denoted in IUGR, which could be interpreted as a hypertrophic compensatory mechanism and is consistent with previous studies from experimental models of severe IUGR (28, 54, 55).

Our current analysis reports cardiomyocyte structural changes induced by IUGR. The stereological estimation of the volume densities of the different cellular components provides evidence that IUGR fetal hearts show a less organized intracellular arrangement, characterized by an increased relative volume occupied by cytoplasm and a decreased relative volume occupied by mitochondria. These changes under IUGR could be due to either alterations on cardiac development or hypoxia, or to mechanical stress caused by pressure or volume overload (49, 53). All the above mechanisms are believed to occur in and contribute to the development of cardiac dysfunction in IUGR, although the exact mechanisms are still not well understood. Recently it has been shown that experimentally induced pressure overload results in a depression of mitochondrial respiratory capacity together with a reduction of total

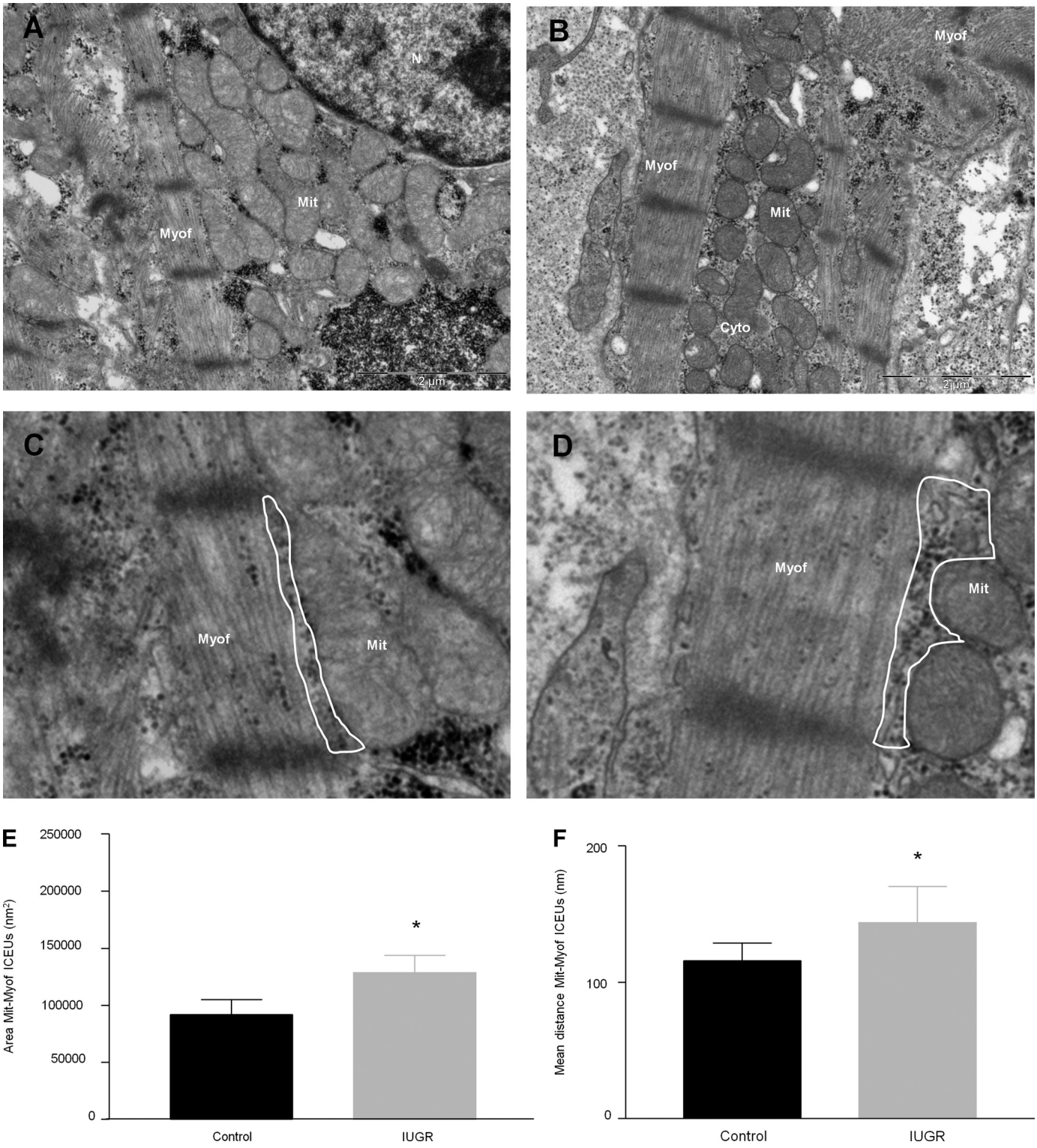

Fig. 4. Arrangement of ICEUs. Representative micrographs show an overview of a mitochondrial network surrounded by myofilaments in a control (*A*) and IUGR (*B*) fetal cardiomyocyte. *C* (control) and *D* (IUGR) are a detail of *A* and *B*, respectively, showing delineated ICEUs. Although in control myocardium mitochondria are closely apposed to myofilaments, the cytoplasmic space between mitochondria and myofilaments is greater in IUGR. *E* and *F*: quantification of the average area of cytoplasm and the mean distance between mitochondria and myofilaments within ICEUs, respectively. $*P < 0.05$. Data in graphs are expressed as means ± SD. Magnification: 20,000×. Scale bar = 2 μm. Mit, mitochondria; Myof, myofilaments; Cyto, cytoplasm; N, nucleus.

Table 2. *Gene set analysis with FatiScan*

Annotation	GO Annotation	Uprepresented in IUGR, %	Downrepresented in IUGR, %	*P* Value	Adjusted *P* Value	GO Type
Oxidative phosphorylation	0006119	1.03	0.17	1.15e-4	7.87e-2*	Biological process
Oxygen homeostasis	0032364	0.49	0.04	1.63e-4	7.82e-2*	Biological process
Mitochondrial respiratory chain complex I	0005747	0.44	0	1.39e-3	7.29e-2*	Cellular component
NADH dehydrogenase	0003954	0.35	0	4.37e-4	6.03e-2*	Molecular function

Gene Ontology (GO) annotations involved in energy production and cardiac energetic metabolism regulation with a statistically significant enrichment in IUGR. *Adjusted *P* value <0.08.

mitochondrial volume density, with a stronger effect on intermyofibrillar (IFM) compared with subsarcolemmal mitochondria (SSM) (42). Because our study samples are fetal, we cannot provide structural and functional differences between IFM and SSM (32). Despite that, our observations of a decrease on mitochondrial relative volume in IUGR are in line with the observations from Schwarzer et al. (42). The resulting structural remodeling shown in Fig. 4 from Schwarzer et al. (42) appears to be very similar to the structural remodeling presented in this study in IUGR hearts (Fig. 4). Additionally, in the same study (42), they relate a decrease in mitochondrial density with a decrease in mitochondrial size, since the citrate synthase activity is decreased in pressure overload but the mitochondrial number is not. We do not observe changes on the number or in the area of individual mitochondria. Since the stereological study shows a decreased relative volume occupied by mitochondria, we hypothesize that smaller mitochondrial size could be the reason for the decreased mitochondrial density (similar to what was described in pressure overloaded hearts) (42), despite the lack of significance, which might be attributed to sample size restrictions. The decrease in mitochondrial density but with no changes in myofibrillar content, as we show, has also been observed in fetal sheep subjected to high altitude hypoxia, which is in agreement with an alteration caused by the lack of oxygen during intrauterine life (27).

Concerning the relative volume occupied by cytoplasm, we observe that the total relative density of cytoplasm is increased in IUGR; however, when it is classified into free cytoplasm or cytoplasm within ICEUs, the former is not significantly increased, whereas the latter is increased in IUGR hearts. We show that both the area of cytoplasm and the mean distance between mitochondria and myofilaments within ICEUs are increased in IUGR myocardium. In fetal heart, energy transfer is believed to rely on the direct ATP and ADP channeling between organelles since the CK-bound (creatine kinase) system is not mature (23). Its efficiency mostly depends on the close interaction between mitochondria and myofilaments (24). In this regard, it has been reported that intracellular disorganization restricts ATP and ADP diffusion, decreasing the efficiency of energy transfer (5). Because ICEUs play a central role in maintaining cardiac energetic homeostasis, alterations on their structure could alter the energy production, utilization, and transfer, and as a consequence, cardiac function could be compromised (45). Based on previous studies, our data suggest that the abnormal arrangement of ICEUs could contribute to the development of less efficient hearts in IUGR, maybe due to a decrease on the energy transfer efficiency from mitochondria to the main cardiac ATPases. Such compromise of cardiac function due to alterations on ICEUs has been previously shown in heart failure (24). The abnormal arrangement of ICEUs in IUGR could also be interpreted as a maturation delay, since it has been described that during cardiac maturation there are major changes on the cardiomyocyte intracellular organization in which mitochondria get closer to myofilament to form the ICEUs (34).

Therefore, from one side our findings present a close similarity to the previously described in experimentally induced pressure overload cardiac dysfunction (18, 42). On the other side, it has been described that cytoarchitectural perturbations can lead to energetic alterations, and conversely perturbations of cellular energetic metabolism can lead to ultrastructural remodeling (52). In our study, it remains uncertain whether the structural changes could contribute to be a cause or a consequence of the cardiac dysfunction previously documented in IUGR.

Subsequently, we wanted to evaluate whether these structural changes are related to subtle changes on gene expression. For this purpose we performed a gene expression microarray experiment, which is complementary to the structural data and provides new evidence regarding the insults that IUGR hearts are receiving. We have used advanced bioinformatics analytic tools based on FatiScan gene set analysis (3), integrated in Babelomics (31). We propose the use of such procedure to scan ordered lists of genes and understand the biological processes operating behind them. Genes were ordered by differential expression between the two experimental conditions. There were not individual genes with significant differential expression. The output result of the differential expression analysis (ranked list by the statistic of the test) was the input for the gene set analysis. On this full list of genes, Fatiscan detected groups of genes with the same expression pattern and sharing biological functions. Therefore, the same analysis evaluated IUGR group and control group at the same time. Our analysis identified key gene pathways related to cardiac energy production, which were compromised under IUGR. This included oxygen homeostasis (GO: 0032364), oxidative phosphorylation (GO: 0006119), mitochondrial respiratory chain complex I (GO: 0005747), and NADH dehydrogenase activity (GO: 0003954). On one hand, alterations on the oxygen homeostasis and oxidative phosphorylation suggest that IUGR hearts are suffering from hypoxia. Previous studies have shown a 20–35% decrease in the oxidative phosphorylation in skeletal muscle from IUGR rats, leading to a decrease in ATP production and thus an impairment of skeletal muscle function (43). Additionally, exposure to chronic hypoxia has been related to a decrease in cardiac oxidative capacity in rats, which leads to a decline in ATP synthesis and in oxygen consumption (2). Hypoxia during early life has also been associated to persistent changes in genes linked to the regulation of cardiac metabolic processes that remain present long after the termina-

tion of the neonatal hypoxic insult (15). This may eventually be linked to the cardiovascular programming due to IUGR and the long-term persistence of the changes. On the other hand, alterations on the expression of mitochondrial respiratory chain complex I and specifically on the NADH dehydrogenase activity are again in line with the study of Schwarzer et al. (42) in pressure overload, in which they observe decreased function of the mitochondrial respiratory chain complex I. Our observations are also consistent with other studies in human IUGR in which a deficiency of the mitochondrial respiratory chain complex I has been observed (19).

Several study limitations and technical considerations should be mentioned. The morphological characterization of cardiomyocyte intracellular organization and ICEUs only provides structural information. Further studies are required to elucidate the functional consequences of these alterations. The bioinformatics gene set analysis used in this study is useful for studying diseases in which subtle differences are expected to occur, like in IUGR. Therefore, rather than expression changes on individual genes, alterations are expected to occur at the level of biological pathways and functionally related groups of genes. IUGR is thought to be a multifactorial disease in which several pathways and multiple members of a pathway might be involved, often resulting in only subclinical changes. However, we acknowledge that it is difficult to address the actual biological relevance of the gene expression findings. Future functional studies are required to relate the gene expression changes to the functional alterations at the cellular level. Finally, we do not evaluate the postnatal persistence in this study, which would provide valuable data of the long-term impact of the changes. However, this goal lies beyond the scope of the present study and should be investigated in future research.

In conclusion, we demonstrate that hearts from IUGR fetuses present a less organized intracellular arrangement of the cardiomyocyte organelles. These structural changes are accompanied with differences in the expression of groups of genes related to energy production and oxygen homeostasis. Overall, this study suggests that energetic metabolism is impaired in IUGR and provides new evidence to characterize cellular and subcellular mechanisms underlying cardiac remodeling in IUGR. Our findings might help to explain the global cardiac dysfunction previously documented in IUGR fetuses and children, and deserve further investigation to ascertain long-term persistence as part of the cardiovascular programming observed in IUGR.

ACKNOWLEDGMENTS

We thank Carmen López-Iglesias, head of the electron cryo-microscopy unit of CCiTUB (Centres Científics i Tecnològics de la Universitat de Barcelona), for support and advice with electron microscopy techniques.

GRANTS

This study was supported by grants from Ministerio de Economia y Competitividad PN de I+D+I 2008-2011 (ref. SAF2009_08815); Instituto de Salud Carlos III (ref. PI11/00051, PI11/01709) cofinanciado por el Fondo Europeo de Desarrollo Regional de la Unión Europea "Una manera de hacer Europa"; Centro para el Desarrollo Técnico Industrial (Ref. cvREMOD 2009-2012) apoyado por el Ministerio de Economia y Competitividad y Fondo de inversión local para el empleo, Spain; and AGAUR 2009 SGR Grant No. 1099. I. Torre was supported by a postdoctoral fellowship from Carlos III Institute of Health (Spain) (CD08/00176). P. Garcia-Canadilla acknowledges grant support to the Programa de Ayudas Predoctorales de Formación en Investigación en Salud del Instituto Carlos III, Spain (FI12/00362). A. Gonzalez-Tendero was supported by an IDIBAPS (Institut d'Investigacions Biomèdiques August Pi i Sunyer) predoctoral fellowship.

DISCLOSURES

No conflicts of interest, financial or otherwise, are declared by the author(s).

AUTHOR CONTRIBUTIONS

Author contributions: A.G.-T., I.T., F.C., and E.G. conception and design of research; A.G.-T., I.T., F.G.-G., and J.D. performed experiments; A.G.-T., I.T., P.G.-C., F.G.-G., and J.D. analyzed data; A.G.-T., I.T., F.C., B.B., and E.G. interpreted results of experiments; A.G.-T. prepared figures; A.G.-T. drafted manuscript; A.G.-T., I.T., F.C., B.B., and E.G. edited and revised manuscript; all authors approved final version of manuscript.

REFERENCES

1. **Alberry M, Soothill P.** Management of fetal growth restriction. *Arch Dis Child Fetal Neonatal Ed* 92: F62–F67, 2007.
2. **Al Ghouleh I, Khoo NK, Knaus UG, Griendling KK, Touyz RM, Thannickal VJ, Barchowsky A, Nauseef WM, Kelley EE, Bauer PM, Darley-Usmar V, Shiva S, Cifuentes-Pagano E, Freeman BA, Gladwin MT, Pagano PJ.** Oxidases and peroxidases in cardiovascular and lung disease: new concepts in reactive oxygen species signaling. *Free Radic Biol Med* 51: 1271–1288, 2011.
3. **Al-Shahrour F, Arbiza L, Dopazo H, Huerta-Cepas J, Mínguez P, Montaner D, Dopazo J.** From genes to functional classes in the study of biological systems. *BMC Bioinformatics* 8: 114, 2007.
4. **Al-Shahrour F, Carbonell J, Minguez P, Goetz S, Conesa A, Tárraga J, Medina I, Alloza E, Montaner D, Dopazo J.** Babelomics: advanced functional profiling of transcriptomics, proteomics and genomics experiments. *Nucleic Acids Res* 36: W341–W346, 2008.
5. **Anmann T, Guzun R, Beraud N, Pelloux S, Kuznetsov AV, Kogerman L, Kaambre T, Sikk P, Paju K, Peet N, Seppet E, Ojeda C, Tourneur Y, Saks V.** Different kinetics of the regulation of respiration in permeabilized cardiomyocytes and in HL-1 cardiac cells. Importance of cell structure/organization for respiration regulation. *Biochim Biophys Acta* 1757: 1597–1606, 2006.
6. **Bae S, Xiao Y, Li G, Casiano CA, Zhang L.** Effect of maternal chronic hypoxic exposure during gestation on apoptosis in fetal rat heart. *Am J Physiol Heart Circ Physiol* 285: H983–H990, 2003.
7. **Barker DJ.** Fetal origins of cardiovascular disease. *Ann Med* 1: 3–6, 1999.
8. **Bassan H, Trejo LL, Kariv N, Bassan M, Berger E, Fattal A, Gozes I, Harel S.** Experimental intrauterine growth retardation alters renal development. *Pediatr Nephrol* 15: 192–195, 2000.
9. **Beaudoin S, Barbet P, Bargy F.** Developmental stages in the rabbit embryo: guidelines to choose an appropriate experimental model. *Fetal Diagn Ther* 18: 422–427, 2003.
10. **Benjamini Y, Hochberg Y.** Controlling the false discovery rate a practical and powerful approach to multiple testing. *J R Statist Soc B* 57: 289–300, 1995.
11. **Breu H, Gil J, David Kirkpatrick D, Werman M.** Linear time Euclidean distance transform algorithms. *IEEE Trans Pattern Anal Mach Intell* 5: 529–533, 1995.
12. **Comas M, Crispi F, Cruz-Martinez R, Martinez JM, Figueras F, Gratacos E.** Usefulness of myocardial tissue Doppler vs. conventional echocardiography in the evaluation of cardiac dysfunction in early-onset intrauterine growth restriction. *Am J Obstet Gynecol* 203: e1–e7, 2010.
13. **Crispi F, Bijnens B, Figueras F, Bartrons J, Eixarch E, Le Noble F, Ahmed A, Gratacós E.** Fetal growth restriction results in remodeled and less efficient hearts in children. *Circulation* 121: 2427–2436, 2010.
14. **Crispi F, Hernandez-Andrade E, Pelsers MM, Plasencia W, Benavides-Serralde JA, Eixarch E, Le Noble F, Ahmed A, Glatz JF, Nicolaides KH, Gratacos E.** Cardiac dysfunction and cell damage across clinical stages of severity in growth-restricted fetuses. *Am J Obstet Gynecol* 199: e1–e8, 2008.
15. **Del Duca D, Tadevosyan A, Karbassi F, Akhavein F, Vaniotis G, Rodaros D, Villeneuve LR, Allen BG, Nattel S, Rohlicek CV, Hébert TE.** Hypoxia in early life is associated with lasting changes in left ventricular structure and function at maturity in the rat. *Int J Cardiol* 156: 165–173, 2012.
16. **Eixarch E, Figueras F, Hernández-Andrade E, Crispi F, Nadal A, Torre I, Oliveira S, Gratacós E.** An experimental model of fetal growth restriction based on selective ligature of uteroplacental vessels in the pregnant rabbit. *Fetal Diagn Ther* 26: 203–211, 2009.
17. **Eixarch E, Hernandez-Andrade E, Crispi F, Illa M, Torre I, Figueras F, Gratacos E.** Impact on fetal mortality and cardiovascular Doppler of

selective ligature of uteroplacental vessels compared with undernutrition in a rabbit model of intrauterine growth restriction. *Placenta* 32: 304–309, 2011.
18. **Friehs I, Cowan DB, Choi YH, Black KM, Barnett R, Bhasin MK, Daly C, Dillon SJ, Libermann TA, McGowan FX, del Nido PJ, Levitsky S, McCully JD.** Pressure-overload hypertrophy of the developing heart reveals activation of divergent gene and protein pathways in the left and right ventricular myocardium. *Am J Physiol Heart Circ Physiol* 304: H697–H708, 2013.
19. **Gibson K, Halliday JL, Kirby DM, Yaplito-Lee J, Thorburn DR, Boneh A.** Mitochondrial oxidative phosphorylation disorders presenting in neonates: clinical manifestations and enzymatic and molecular diagnoses. *Pediatrics* 122: 1003–1008, 2008.
20. **Gundersen HJ, Bendtsen TF, Korbo L, Marcussen N, Møller A, Nielsen K, Nyengaard JR, Pakkenberg B, Sørensen FB, Vesterby A, West MJ.** Some new, simple and efficient stereological methods and their use in pathological research and diagnosis. *APMIS* 96: 379–394, 1988.
21. **Hecher K, Snijders R, Campbell S, Nicolaides K.** Fetal venous, intracardiac, and arterial blood flow measurements in intrauterine growth retardation: relationship with fetal blood gases. *Am J Obstet Gynecol* 173: 10–15, 1995.
22. **Hiraumi Y, Iwai-Kanai E, Baba S, Yui Y, Kamitsuji Y, Mizushima Y, Matsubara H, Watanabe M, Watanabe K, Toyokuni S, Matsubara H, Nakahata T, Adachi S.** Granulocyte colony-stimulating factor protects cardiac mitochondria in the early phase of cardiac injury. *Am J Physiol* 29: 823–832, 2009.
23. **Hoerter JA, Kuznetsov A, Ventura-Clapier R.** Functional development of the creatine kinase system in perinatal rabbit heart. *Circ Res* 69: 665–676, 1991.
24. **Joubert F, Wilding JR, Fortin D, Domergue-Dupont V, Novotova M, Ventura-Clapier R, Veksler V.** Local energetic regulation of sarcoplasmic and myosin ATPase is differently impaired in rats with heart failure. *J Physiol* 586: 5181–5192, 2008.
25. **Kanaka-Gantenbein C.** Fetal origins of adult diabetes. *Ann N Y Acad Sci* 1205: 99–105, 2010.
26. **Lemieux H, Semsroth S, Antretter H, Höfer D, Gnaiger E.** Mitochondrial respiratory control and early defects of oxidative phosphorylation in the failing human heart. *Int J Biochem Cell Biol* 43: 1729–1738, 2011.
27. **Lewis AM, Mathieu-Costello O, McMillan PJ, Gilbert RD.** Quantitative electron microscopic study of the hypoxic fetal sheep heart. *Anat Rec* 256: 381–388, 1999.
28. **Lim K, Zimanyi MA, Black MJ.** Effect of maternal protein restriction during pregnancy and lactation on the number of cardiomyocytes in the postproliferative weanling rat heart. *Anat Rec (Hoboken)* 293: 431–437, 2010.
29. **Lopaschuk GD, Jaswal JS.** Energy metabolic phenotype of the cardiomyocyte during development, differentiation, and postnatal maturation. *J Cardiovasc Pharmacol* 56: 130–140, 2010.
30. **The Mathworks Inc.** Mathworks 2007b, version 7.5.0.342. MATLAB. Massachusetts: The MathWorks Inc.
31. **Medina I, Carbonell J, Pulido L, Madeira SC, Goetz S, Conesa A, Tárraga J, Pascual-Montano A, Nogales-Cadenas R, Santoyo J, García F, Marbà M, Montaner D, Dopazo J.** Babelomics: an integrative platform for the analysis of transcriptomics, proteomics and genomic data with advanced functional profiling. *Nucleic Acids Res* 38: W210–W213, 2010.
32. **Nassar R, Reedy MC, Anderson PA.** Developmental changes in the ultrastructure and sarcomere shortening of the isolated rabbit ventricular myocyte. *Circ Res* 61: 465–483, 1987.
33. **Nouette-Gaulain K, Malgat M, Rocher C, Savineau JP, Marthan R, Mazat JP, Sztark F.** Time course of differential mitochondrial energy metabolism adaptation to chronic hypoxia in right and left ventricles. *Cardiovasc Res* 66: 132–140, 2005.
34. **Piquereau J, Novotova M, Fortin D, Garnier A, Ventura-Clapier R, Veksler V, Joubert F.** Postnatal development of mouse heart: formation of energetic microdomains. *J Physiol* 588: 2443–2454, 2010.
35. **Porter GA, Hom J, Hoffman D, Quintanilla R, de Mesy Bentley K, Sheu SS.** Bioenergetics, mitochondria, and cardiac myocyte differentiation. *Prog Pediatr Cardiol* 31: 75–81, 2011.
36. **Rasband WS.** ImageJ. National Institutes of Health, Bethesda, Maryland, USA, http://imagej.nih.gov/ij/, 1997–2011.
37. **Ream M, Ray AM, Chandra R, Chikaraishi DM.** Early fetal hypoxia leads to growth restriction and myocardial thinning. *Am J Physiol Regul Integr Comp Physiol* 295: R583–R595, 2008.
38. **Rueda-Clausen CF, Morton JS, Davidge ST.** Effects of hypoxia-induced intrauterine growth restriction on cardiopulmonary structure and function during adulthood. *Cardiovasc Res* 81: 713–722, 2009.
39. **Rueda-Clausen CF, Morton JS, Lopaschuk GD, Davidge ST.** Long-term effects of intrauterine growth restriction on cardiac metabolism and susceptibility to ischaemia/reperfusion. *Cardiovasc Res* 90: 285–294, 2011.
40. **Saks V, Kuznetsov AV, Gonzalez-Granillo M, Tepp K, Timohhina N, Karu-Varikmaa M, Kaambre T, Dos Santos P, Boucher F, Guzun R.** Intracellular energetic units regulate metabolism in cardiac cells. *J Mol Cell Cardiol* 52: 419–436, 2012.
41. **Scheubel RJ, Tostlebe M, Simm A, Rohrbach S, Prondzinsky R, Gellerich FN, Silber RE, Holtz J.** Dysfunction of mitochondrial respiratory chain complex I in human failing myocardium is not due to disturbed mitochondrial gene expression. *J Am Coll Cardiol* 40: 2174–2181, 2002.
42. **Schwarzer M, Schrepper A, Amorim PA, Doenst T.** Pressure overload differentially affects respiratory capacity in interfibrillar and subsarcolemmal mitochondria. *Am J Physiol Heart Circ Physiol* 304: H529–H537, 2013.
43. **Selak MA, Storey BT, Peterside I, Simmons RA.** Impaired oxidative phosphorylation in skeletal muscle of intrauterine growth-retarded rats. *Am J Physiol Endocrinol Metab* 285: E130–E137, 2003.
44. **Seppet EK, Eimre M, Anmann T, Seppet E, Peet N, Käämbre T, Paju K, Piirsoo A, Kuznetsov AV, Vendelin M, Gellerich FN, Zierz S, Saks VA.** Intracellular energetic units in healthy and diseased hearts. *Exp Clin Cardiol* 10: 173–183, 2005.
45. **Seppet EK, Eimre M, Anmann T, Seppet E, Piirsoo A, Peet N, Paju K, Guzun R, Beraud N, Pelloux S, Tourneur Y, Kuznetsov AV, Käämbre T, Sikk P, Saks VA.** Structure-function relationships in the regulation of energy transfer between mitochondria and ATPases in cardiac cells. *Exp Clin Cardiol* 11: 189–194, 2006.
46. **Skilton MK, Evans N, Griffiths KA, Harmer JA, Celermajer D.** Aortic wall thickness in newborns with intrauterine growth restriction. *Lancet* 23: 1484–1486, 2005.
47. **Soothill PW, Nicolaides KH, Campbell S.** Prenatal asphyxia, hyperlacticaemia, hypoglycaemia, and erythroblastosis in growth retarded fetuses. *BMJ* 294: 1051–1053, 1987.
48. **Stanley WC, Recchia FA, Lopaschuk GD.** Myocardial substrate metabolism in the normal and failing heart. *Physiol Rev* 85: 1093–1129, 2005.
49. **Tintu A, Rouwet E, Verlohren S, Brinkmann J, Ahmad S, Crispi F, van Bilsen M, Carmeliet P, Staff AC, Tjwa M, Cetin I, Gratacos E, Hernandez-Andrade E, Hofstra L, Jacobs M, Lamers WH, Morano I, Safak E, Ahmed A, le Noble F.** Hypoxia induces dilated cardiomyopathy in the chick embryo: mechanism, intervention, and long-term consequences. *PLos One* 4: e5155, 2009.
50. **Tong W, Xue Q, Li Y, Zhang L.** Maternal hypoxia alters matrix metalloproteinase expression patterns and causes cardiac remodeling in fetal and neonatal rats. *Am J Physiol Heart Circ Physiol* 301: H2113–H2121, 2011.
51. **Turan S, Turan OM, Salim M, Berg C, Gembruch U, Harman CR, Baschat AA.** Cardiovascular transition to extrauterine life in growth-restricted neonates: relationship with prenatal Doppler findings. *Fetal Diagn Ther* 33: 103–109, 2013.
52. **Ventura-Clapier R, Garnier A, Veksler V, Joubert F.** Bioenergetics of the failing heart. *Biochim Biophys Acta* 1813: 1360–1372, 2011.
53. **Verburg BO, Jaddoe VW, Wladimiroff JW, Hofman A, Witteman JC, Steegers EA.** Fetal hemodynamic adaptive changes related to intrauterine growth: the Generation R Study. *Circulation* 117: 649–659, 2008.
54. **Wang KC, Zhang L, McMillen IC, Botting KJ, Duffield JA, Zhang S, Suter CM, Brooks DA, Morrison JL.** Fetal growth restriction and the programming of heart growth and cardiac insulin-like growth factor 2 expression in the lamb. *J Physiol* 589: 4709–4722, 2011.
55. **Xu Y, Williams SJ, O'Brien D, Davidge ST.** Hypoxia or nutrient restriction during pregnancy in rats leads to progressive cardiac remodeling and impairs postischemic recovery in adult male offspring. *FASEB J* 20: 1251–1253, 2006.